Chinese Journal of Polymer Science Vol. 33, No. 4, (2015), 633–645

Chinese Journal of Polymer Science
© Chinese Chemical Society
Institute of Chemistry, CAS
Springer-Verlag Berlin Heidelberg 2015

Reconstruction of Core-Shell Dispersed Particles in Impact Polypropylene Copolymer during Extrusion*

Feng Chen, Bi-wei Qiu, Ya-nan Ye, Yu-hua Lv, Yong-gang Shangguan**, Yi-hu Song and Qiang Zheng**

MOE Key Laboratory of Macromolecular Synthesis and Functionalization, Department of Polymer Science and Engineering, Zhejiang University, Hangzhou 310027, China

Abstract We reported an approach to reconstruct the complex phase morphology of impact polypropylene copolymer (IPC) with core-shell dispersed particles and to optimize its toughness in approximate shear condition. The molten-state annealing results indicate that the phase structure with core-shell dispersed particles is unstable and could be completely destroyed by static annealing, resulting in the degradation of impact strength. By using a co-rotating twin screw extruder, we found that the dispersed particle with core-shell structure could be rebuilt in appropriate condition with the recovery of excellent impact strength due to both the huge interfacial tension during solidification and the great difference in viscosity of components. Results reveal that almost all the extruded IPCs show the impact strength 60%–90% higher than that of annealed IPCs at room temperature. And the twice-extruded IPC shows the highest impact strength, 446% higher than that of IPC annealed for 30 min. As for low temperature tests, the impact strength of extruded IPCs also increases by 33%–58%. According to adjusting the processing conditions including extrusion speed, extrusion frequency and temperature, an optimization of toughness was well established.

Keywords: Impact polypropylene copolymer; Shear; Phase morphology; Core-shell dispersed particle; Impact strength.

Electronic Supplementary Material Supplementary material is available in the online version of this article at http://dx.doi.org/10.1007/s10118-015-1616-0.

INTRODUCTION

Although isotactic polypropylene (*i*PP) has been widely applied in many fields due to its good mechanical properties and low cost, it is still restricted in some occasions because of its poor impact strength especially at low temperatures. On account of significance in industry, a great deal of effort has been made to improve the impact property of *i*PP, such as adding a variety of elastomers[1–4], toughening with nanoparticles[5–7] and changing the crystalline form[8, 9], yet it was still unsatisfactory until the appearance of impact polypropylene copolymer (IPC) polymerized by porous spherical $TiCl_4/MgCl_2$ catalyst[10]. IPC is an *in situ* copolymer, also called polypropylene catalloy (PP-cat) or high-impact polypropylene (HIPP), which is produced by two-step polymerization including homo-polymerization of propylene and subsequent copolymerization of propylene and ethylene in a gas-phase reactor by using a special Ziegler-Natta catalyst[11]. The special copolymerization technique causes IPC to be a multi-phase and multi-component polymeric material with excellent impact

* This work was financially supported by the National Natural Science Foundation of China (Nos. 51173157 and 51173165) and the Fundamental Research Funds for the Central Universities (No. 2013QNA4048).
** Corresponding authors: Yong-gang Shangguan (上官勇刚), E-mail: shangguan@zju.edu.cn
Qiang Zheng (郑强), E-mail: zhengqiang@zju.edu.cn
Received August 12, 2014; Revised September 12, 2014; Accepted January 5, 2015
doi: 10.1007/s10118-015-1616-0

property, especially at low temperatures, and subsequently it becomes an important commercial polyolefin used in many applications.

Many works have been made to investigate the composition[12, 13], morphology and structure[14, 15], crystallization behavior[15–18], mechanical properties[19, 20] and rheological behavior[21, 22] of IPC. Based on these works, the composition of IPC has been expounded clearly and it mainly contains three components, *i.e.*, ethylene-propylene random copolymer (EPR), a series of ethylene propylene block copolymers with different sequence lengths (E*b*P) and propylene homopolymer (hPP). However, a small amount of ethylene homopolymer (hPE) was also found in certain IPC[23]. According to solvent extraction, scanning electron microscope (SEM) and transmission electron microscope (TEM) observations, we[16, 24] have proposed a dispersed phase model for IPC with multilayered core-shell structure. In this model, the dispersed particle is composed of an E*b*P core and two layers including the outer E*b*P layer and the inner EPR one. In particular, some E*b*P passes through the EPR layer and forms some bridges connecting the core and E*b*P layer. Some other researchers[17, 18, 25, 26] also demonstrated similar phase structure models for IPC: apart from a slight difference that whether there is some hPE in the core, these models are almost identical.

To investigate the relationship between structure and property of IPC, many works have been conducted in recent years[19, 20, 27–30]. According to investigating two IPCs with almost the same ethylene content, molecular weight and molecular weight distribution[19], it was revealed that poor interfacial adhesion between the dispersed phase and the matrix, larger dimensions and non-uniform distribution of dispersed phase should response to the low impact strength in the IPC possessing a low content of E*b*P component, indicating the important role of E*b*P in exhibiting an excellent mechanical property for IPC. Rungswang[20] revealed the relationship between the microstructure of E*b*P and the mechanical properties of IPC. Results indicated that IPC comprising high content of E*b*P with long homo-PP segment can extend the elongation at break while E*b*P with high content of homo-PE segment contributes to high impact strength. Furthermore, Luo *et al*.[29, 30] studied the temperature dependence of the toughening behavior of β-nucleated IPC. They pointed out that the processing temperature for IPC melt plays an important role in the formation of the morphology after adding the β nucleating agent and established a close correlation between impact strength at 0 °C and chain mobility of the amorphous portion. Moreover, the phase structure and crystallization behavior of IPC after molten-state annealing were also studied systematically[15, 24]. Significantly accelerated crystallization kinetics was found in IPC samples after shear[17, 18], and Song *et al*. proposed that PE segments can gather together to form stable nuclei and play a role to enhance the subsequent crystallization rate of IPC through improving the nucleation rate.

As mentioned above, the extraordinary properties of IPC have been thought to be determined by its unique morphology with core-shell dispersed phase structure. However, it has been found that during processing period, the original phase structure produced by the two-step copolymerization could vary and even coarsen due to thermal and shear effects[15, 27, 28, 31]. It is considerable that the variation in phase structure during processing will give rise to some unexpected changes in properties of product material[32–35]. Moreover, no one can document how the complex phase morphology of IPC forms so far due to the fact that it is an *in situ* polymer alloy. Most of works for developing IPC with more excellent properties focused on the development of new catalytic agent and improving polymerization technology. Although many researches have shown that the excellent properties of IPC strongly depend on its complex phase morphology, the structure-property relationship is scarcely used in fabrication of new IPC because of the unknown mechanism of morphology formation. Thus, to understand the formation of complex phase morphology is important and helpful for fabrication, optimization, stabilization and usage of IPC. Our previous work has studied the influence of long time annealing on morphology of IPC and found the phase inversion phenomenon after annealing at 200 °C for 200 min[15]. However, short time annealing is more practical in industry. And here, we focus on the influence of short time annealing on the morphology and also the impact strength.

According to investigating the evolutions of phase morphology and the corresponding impact properties of IPC during melt annealing, we revealed the influence of phase structure on impact property. More importantly, through adjusting the processing condition, the core-shell dispersed phase structure in IPC which has destroyed

by annealing was successfully reconstructed in a co-rotating twin screw extruder. Subsequently, the critical shear condition of reconstructing core-shell dispersed phase structure was proposed respectively.

EXPERIMENTAL

Materials and Sample Preparation

The commercial IPC (SP179, molar percentage of ethylene component is about 13.5%) was purchased from SINOPEC Qilu Corporation Ltd., China with $M_w = 1.74 \times 10^5$, $M_w/M_n = 3.96$. The as-received IPC pellets were first annealed at 210 °C for 10, 20 and 30 min in a nitrogen atmosphere oven to obtain the annealed pellet samples. Subsequently, the pellet samples annealed for 30 min were extruded in a co-rotating twin screw extruder (PRISM TSE 16 TC, Thermo Scientific, Waltham, UK) under the designated extrusion conditions for different frequencies, with adding a small amount of antioxidant (Irganox 1010, 0.2% content per extrusion). The extrusion conditions are as follows. (i) The annealed IPC was extruded at 180 °C (all barrel zones) with different screw rotation speeds, *i.e.*, '10r', '20r', '30r' and '40r', respectively, in which the numbers represent rotation speed and "r" represents revolutions per minute (r/min). (ii) The annealed IPC was extruded at 180 °C with 20 r/min for once, twice, three times, four times and five times. (iii) The annealed IPC was extruded at 200 °C and 220 °C with 20 r/min for once and twice. Extruded polymer melt was water quenched, pelletized and dried. Finally, the Charpy impact test specimens with the size 80 mm × 10 mm × 4 mm were prepared by compression molding at 180 °C under 10 MPa for 8 min using the original pellets, annealed samples and extrusion samples.

Impact Strength Test

The notched Charpy impact test was conducted on a Charpy impact test machine (MTS Systems Co. Ltd., China) according to ISO 179-1: 2000. A 45° V shaped notch was made (depth 2 mm) before measurement, and the remaining width of the specimens was 8 mm. The specimens were kept in an environment container at –20 °C and 23 °C for 12 h before test, and then immediately subjected to test. The test result was an average of at least eight specimens.

Morphology Observation

The fracture surface of original and treated IPC samples were obtained at liquid nitrogen and then etched in 50 °C *n*-octane for 4 h to remove the EPR component. Samples were observed using SEM (S-4800, Hitachi, Japan) after being coated with gold-palladium. The operating voltage was 3 kV.

The ultrathin sections were obtained by cutting the molding samples in frozen state and were transferred onto copper grids. A JEM-1230 TEM operated at 90 kV was used and bright-field electron micrographs were obtained.

Differential Scanning Calorimetry and Thermal Gravimetric Analysis Measurements

The thermal behavior of original and annealed IPC samples were examined by using a Q100 differential scanning calorimetry (DSC, TA Instruments Corporation, USA) with nitrogen as purge gas. The samples were first heated to 190 °C and held for 5 min to eliminate previous thermal history, and then cooled down to 40 °C and maintained for 5 min. Finally, the samples were heated to 190 °C again and the heat flow curves were recorded as the thermal behavior. Both the heating and cooling rates in all tests were 10 K/min.

Thermal gravimetric analysis (TGA) was carried out by a Pyris 1 TGA (Perkin-Elmer, USA) instrument at 210 °C under nitrogen atmosphere.

Attenuated Total Internal Reflectance Fourier Transform Infrared Spectroscopy Analysis

Samples were prepared as films with thickness of about 200 μm through compression molding and investigated by attenuated total internal reflectance Fourier transform infrared spectroscopy (ATR-FTIR) on a Nicolet 6700 (Thermo Fisher Scientific LLC, USA).

Gel Permeation Chromatography Measurements

Molecular weight distributions for original and treated IPC samples were determined by gel permeation chromatography (GPC) at 150 °C. The GPC system used is a PL-GPC220 equipped with three PLgel 10 mm MIXED-B columns using polystyrene as standards and 1,2,4-trichlorobenzene (1.0 mL/min) as the eluent.

RESULTS AND DISCUSSION

Influence of Annealing on Phase Structure of IPC

As mentioned above, IPC is a multi-component system and presents complicated core-shell dispersed particles. A uniform dispersion in IPC pellet is observed, as shown in Fig. 1, and the core-shell structure is presented in illustration and documented in a previous article in detail[24]. The dispersed phase can present three different cases depending on the degree of wrapping E*b*P core in the EPR layer: (i) isolated holes marked as 'A', (ii) the holes but containing a smaller granule marked as 'B', and (iii) aggregate granules marked as 'D'. It should be pointed out that in the case of E*b*P bridges only exist on the other side away from the viewer, an isolated E*b*P granule is left behind marked as 'C' by removing the outer EPR layer. The partial enlargement of dispersed particle accords with the phase structure model well. Figure 2 gives the morphology micrographs of IPC samples annealed at 210 °C for different time lengths. Similar to original IPC, a three-phase structure can be observed in SEM images for all four samples: besides the hPP matrix, the aggregate granules are comprised of E*b*P component according to the phase model and the holes indicate the removed EPR particles. It can be seen that the good dispersion of dispersed particles with core-shell structure in original pellets is generally destroyed as annealing. The phase domains coarsen with increasing the annealing time. E*b*P granules gradually form a network structure throughout the whole material for samples annealed for 20 and 30 min, whereas the EPR holes grow so slowly compared to E*b*P. Noted that the morphology evolution in IPC is different from that in ordinary *i*PP/EPR binary blends[15], the difference in coarsening of EPR and E*b*P components may be the main reason, which will be investigated systematically in future.

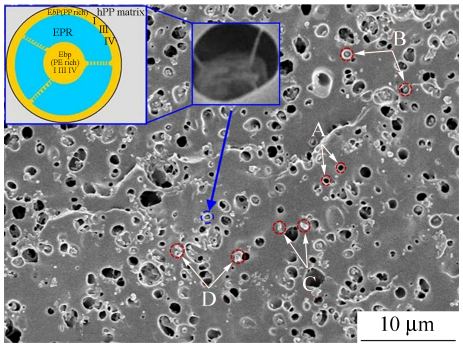


Fig. 1 SEM micrograph of IPC and phase structure model of dispersed phase

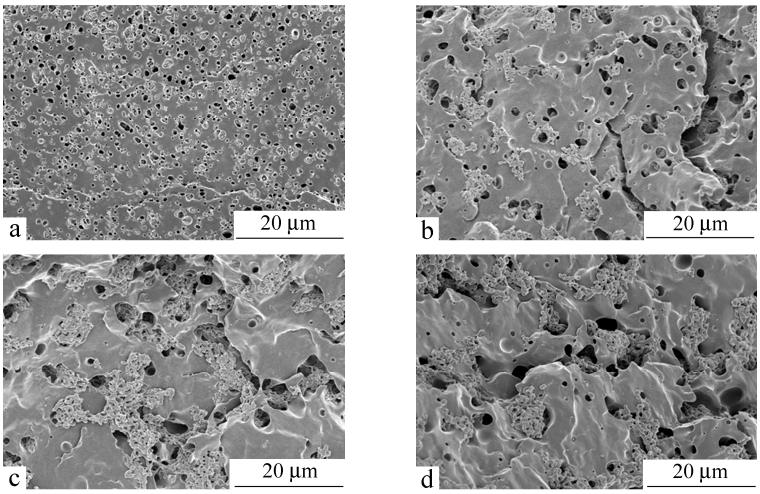


Fig. 2 SEM images of IPC samples annealed at 210 °C for different time: (a) 0 min, (b) 10 min, (c) 20 min and (d) 30 min

Impact Strength of IPC with Different Phase Structure

It is reasonable that the destruction of dispersed phase structure in IPC after annealing would affect its mechanical property. Figure 3(a) gives the notched Charpy impact strength of IPC samples annealed at 210 °C. The statistical results of dispersed phase size in IPC samples are shown in Fig. 3(b). The results were obtained by counting the size of dispersed phase in SEM images. As for counting the E*b*P phase size, SEM images of IPC etched at 50 °C were used. However, SEM images of IPC etched at 100 °C were used to count the EPR phase size since E*b*P could be removed after being etched at 100 °C and the interference of E*b*P granules could be eliminated. The corresponding SEM images of IPC etched at different temperatures are given in Supporting Information.

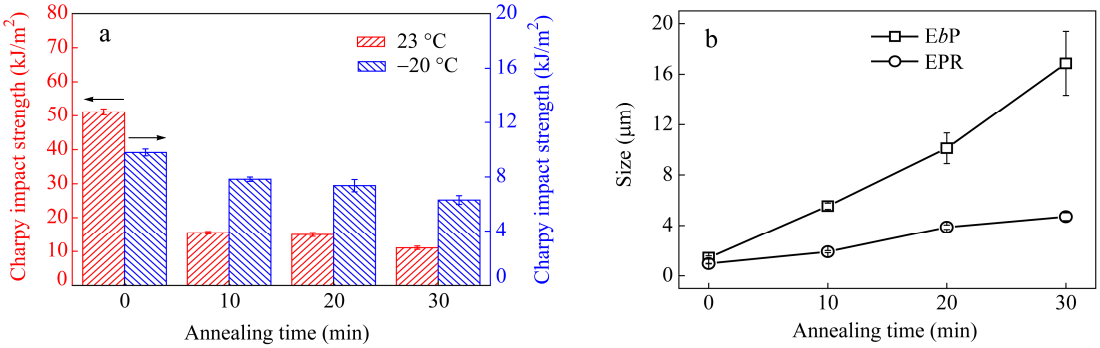


Fig. 3 (a) Notched Charpy impact strength and (b) dispersed phase size of IPC samples annealed at 210 °C for different time lengths

As increasing the annealing time, phase domains of EPR and E*b*P are both gradually coarsen and aggregate granules appear. Furthermore, compared with original IPC, the impact strengths tested at 23 °C and –20 °C for the sample subjected to 10 min annealing decrease substantially. It can be seen from Fig. 3(a) that the impact strength further decreases with increasing the annealing time. It is believed that every rubber-toughened plastic system should possess a critical rubbery particle size for craze nucleation[36, 37]. And the rubbery phase with smaller average particle diameter d seems to be more efficient in toughening PP system[38]. Taking the phase morphology evolution of IPC into account, it is reasonable to ascribe the drop of impact strength during annealing to the destruction of core-shell structure and gathering of rubbery phase.

Since the changes in chemical structure including degradation and crosslinking may take place under high temperatures[21], it is necessary to examine the chemical structure of IPC during annealing due to the influence of the changes in chemical structure on the property of IPC. The previous studies[39–41] on oxidative degradation of PP revealed that carbonyl groups will be produced and the absorption peak at about 1715 cm^{-1} can be observed by infrared spectrometer. ATR-FTIR results (shown in the Supporting Information) confirm that no oxidative degradation occurs in annealed samples due to the protection of nitrogen atmosphere. Furthermore, the GPC and TGA results presented in the Supporting Information, also confirm that there is scarcely any thermal degradation during annealing and the molecular weight distribution has only a very minor change, indicating that changes of chemical structure can be ignored in this annealing process. Moreover, the GPC results shown in Supporting Information also give the molecular weight distribution of IPC after multiple extrusions. Results reveal that molecular weight distribution of IPC exhibits a small change after multiple extrusions, meaning that the influence of changes in molecular weight can be indeed ignored during the whole discussion in this paper.

For crystalline polymer, the crystalline structure is another factor affecting the mechanical properties. It has been documented that the annealing may actually influence the crystallization behavior and the resulting crystalline structure, and in turn affects the mechanical properties of crystalline polymers[42]. Therefore, it is necessary to identify that whether the annealing affects the crystalline structure of IPC. The melting curves of IPC samples annealed for different time lengths are depicted in the Supporting Information. It can be observed

that there is no obvious difference in both crystallinity and lamellar thickness for the four IPC samples, meaning the drop of impact strength is independent of crystalline structure in this case. Consequently, it is reasonable to conclude that the reduction of impact strength for annealed IPC should be ascribed to the variation of phase structure. These results confirm the deduction that the excellent properties of IPC originate from its morphology structure.

As mentioned above, the EPR phase with a good dispersion and small particle size has a significant toughening effect for PP matrix. In the case of IPC, the inner core (mainly comprised of E*b*P component) and the intermediary EPR layer may look as a toughening particle with certain degree of rigidity in this multi-component system. The outer layer (E*b*P) indeed acts as a compatibilizer improving the interfacial interaction between EPR and PP matrix[24, 26]. As a result, the cooperative action between the E*b*P/EPR particle and the compatibilizer (outer E*b*P layer) makes IPC exhibit a good rigidity-toughness balance. During annealing, the core-shell structure is destroyed with the gathering of rubbery phase regions. These two factors are both responsible for the decline of impact strength.

Shear-induced Phase Morphology Reconstruction of IPC

The above results reveal that the impact strength of annealed IPC samples strongly depends on the phase structure. Since the reconstruction of the core-shell structure in IPC has been conducted at an appropriate condition by solution casting[18, 25], it is worthy to explore whether the core-shell structure can revive in melt processing after being destroyed. Figure 4 gives the corresponding SEM images for IPC samples extruded at different screw rotation speeds, in which "IPC-o" stands for the original IPC, "IPC-a" stands for the sample annealed at 210 °C for 30 min. The extruded IPCs are defined as '10r', '20r', '30r' and '40r', respectively. It can be seen that the size of dispersed particles for extruded samples seems to decrease compared with that of IPC-a, but is still larger than that of IPC-o.

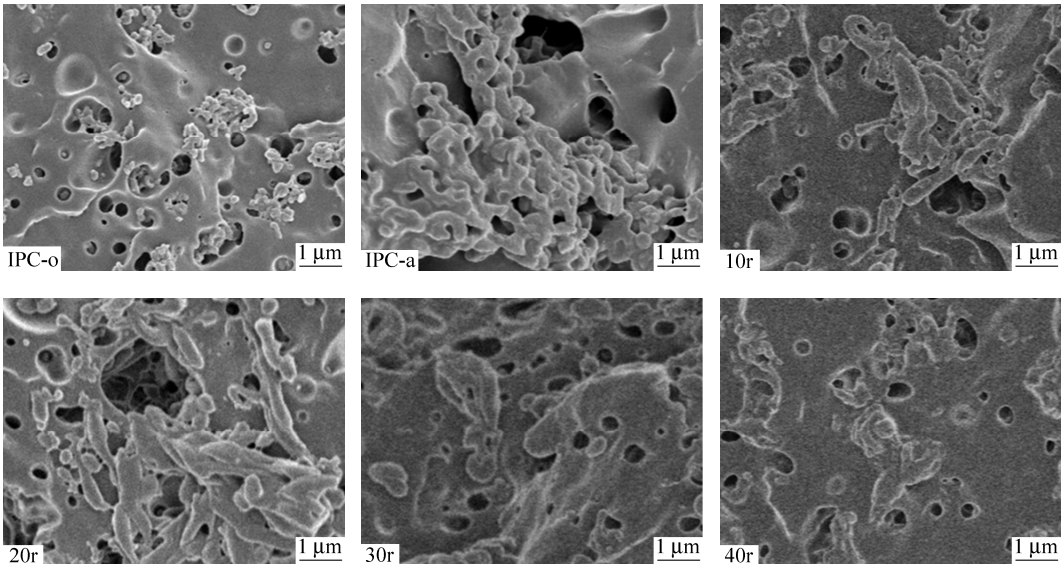


Fig. 4 SEM images for IPC-o, IPC-a and samples extruded with different rotation speeds

Figure 5 gives the SEM images for IPC samples extruded at different frequencies, in which '1t' represent samples extruded once, and the rest can be deduced by analogy. Through comparing the SEM images of extruded samples with IPC-a in Fig. 4 and Fig. 5, it can be seen that both the sizes of E*b*P and EPR phase in extruded samples are smaller than those of IPC-a. Moreover, as seen in SEM images shown in Fig. 5, it is amazing that the phase morphology of the twice-extruded sample is almost the same as that of the original IPC. In order to obtain a whole comparison, SEM and TEM images in larger scale for original and twice-extruded IPC

are presented in Fig. 6. From SEM images in Fig. 6, it can be seen that the amount of structure 'A', 'B' and 'C' in twice-extruded sample is close to that in original IPC. Taking these structures 'A', 'B' and 'C' resulting from the original core-shell structure into account, it is believed the unique dispersed phase structure has partly been reconstructed in the twice-extruded sample. And the corresponding TEM images are also shown in Fig. 6. Here, staining was not conducted in order to preserve the original information about delicate structures, and the contrast resulted from the differences in density[31]. As shown in the TEM images, PE crystals show a stronger contrast than PP crystals, while the amorphous EPR has the weakest contrast. Moreover, the core-shell dispersed particles can be observed in both two samples, marked as arrows. However, the size of core-shell particles in twice-extruded sample seems a little larger than that of original IPC.

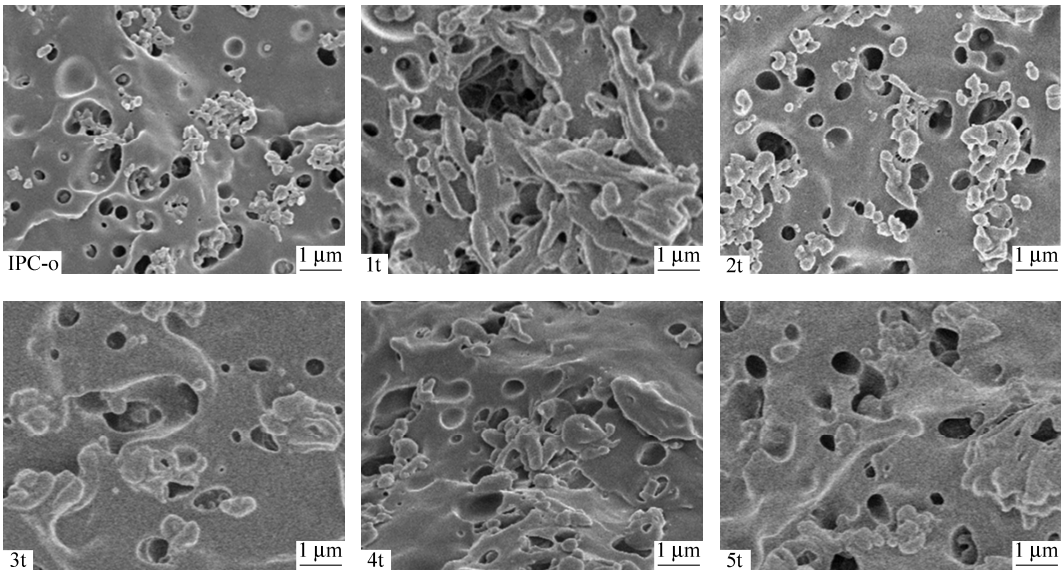


Fig. 5 SEM images for IPC-o and samples extruded at different frequencies

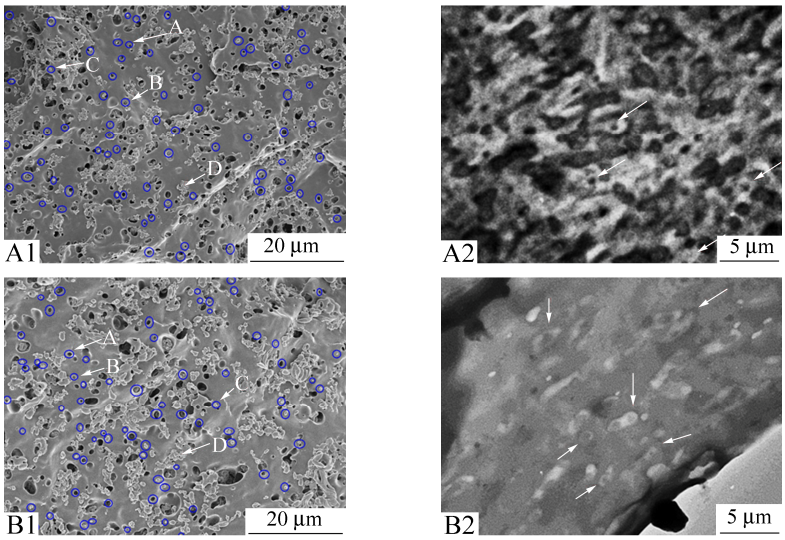


Fig. 6 (1) SEM images and (2) TEM images of (A) original IPC and (B) twice-extruded IPC

In the case of extrusion, there are two opposite issues: phase coarsening induced by thermal effect and dispersing induced by shear. According to changing the extrusion conditions consisting of extrusion temperature

representing thermal effect and screw rotation speed representing shearing strength, a combined effect of them on IPC can result in different phase structures. Furthermore, to some extent increasing extrusion frequency is equal to increasing the extrusion time without decreasing the screw speed, indicating increasing extrusion frequency can make the combined effect be more significant. When the two competing factors reach an appropriate point, both E*b*P and EPR in IPC present a good distribution. Consequently, during solidification, the huge interfacial tension and large difference in viscosity of components may facilitate the reconstruction of core-shell particles similar to that in solution-mixed samples. However, the size of aggregate granules marked as 'D' coming from the destroyed core-shell particles is slightly larger than that in original IPC. It is understandable that the thermal effect always makes phase domains coarsen.

Figure 7 gives impact strength of different samples. As shown in Fig. 7(a), all the impact strengths of extruded samples are significantly higher than those of IPC-a at both two test temperatures. For the test at 23 °C, the impact strength of extruded samples is up to 18.5–21.4 kJ/m^2, 60%–90% higher than that of IPC-a (11.1 kJ/m^2), however it is still far lower than that of original IPC (51.1 kJ/m^2). As for the –20 °C test, the impact strength of extrusion samples also increases by 33%–58%, and in particular the sample extruded at 20r presents approximately identical impact strength with that of original IPC (9.8 kJ/m^2), meaning that the extrusion may eliminate the influence of annealing on impact strength at low temperatures, however partially eliminate at room temperature. It has been pointed out that for IPC, the impact strength is dominated by chain mobility of rubbery phase and amorphous portion of hPP matrix phase[29], indicating the reason for recovery of impact strength may be concerned with the variation of rubbery particle size.

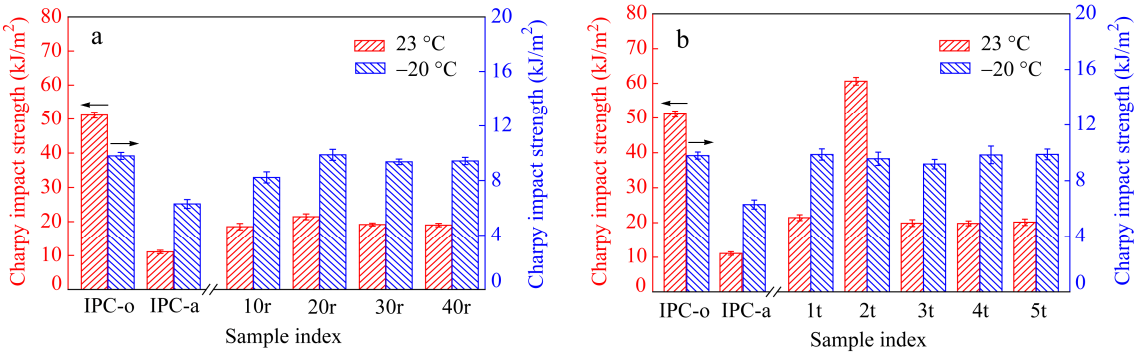


Fig. 7 Notched Charpy impact strength of different IPC samples

Figure 7(b) gives the toughness of IPC samples extruded at different frequencies. As for the 23 °C test, the twice-extruded sample exhibits the highest impact strength which even obviously higher than that of original IPC, indicating that extrusion processing completely eliminates the depression of impact strength resulting from annealing. However, in the cases of being extruded more than twice, the impact strength drops again and generally tends to a constant. It is noted that the definite value of impact strength is still almost 80% higher than that of IPC-a, although it is lower than that of original sample. Differing from the sharp changes of impact strength at 23 °C, the impact strength results measured at –20 °C indicate that all the IPC samples subjected to different extrusion frequencies appear complete recovery in impact strength and the extrusion frequency seems not to influence the recovery effect. Considering the fact that impact strength of the original IPC at low temperatures shows a significant lower value than that at room temperature, just only a small elevation can offset the drop of impact strength resulting from annealing process. That means the impact strength is recovered much quickly at low temperatures than at room temperature. Noted the above results in Fig. 6 that the core-shell dispersed particle has been rebuilt in the twice-extruded sample, the recovery of the impact strength can be ascribed to the reconstruction of the phase structure with core-shell dispersed particles.

In addition, the influence of extrusion temperature on phase morphology of IPC was also investigated.

Figure 8 gives the SEM images of samples extruded at 180 °C, 200 °C and 220 °C, 20 r/min, in which "180-1" stands for being extruded at 180 °C once, and the rest can be deduced by analogy. And Fig. 9 also gives the corresponding impact strength of the different IPC samples. From Fig. 8, a larger size of rubbery particles resulting from the thermal effect at higher temperatures can be observed. Because of mismatching between thermal effects and shear conditions, the core-shell particles are no longer rebuilt even for the twice-extruded samples at 200 °C and 220 °C. Consequently, the impact strengths at both 23 °C and –20 °C of samples extruded at 200 °C and 220 °C are lower than those of samples extruded at 180 °C, respectively, as shown in Fig. 9.

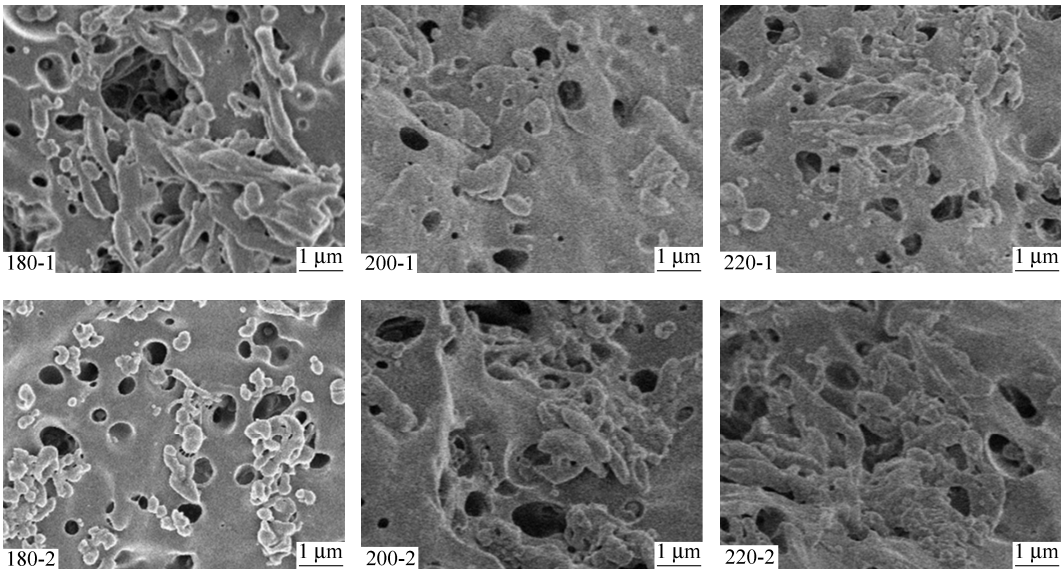


Fig. 8 SEM images for IPC samples extruded at different temperatures

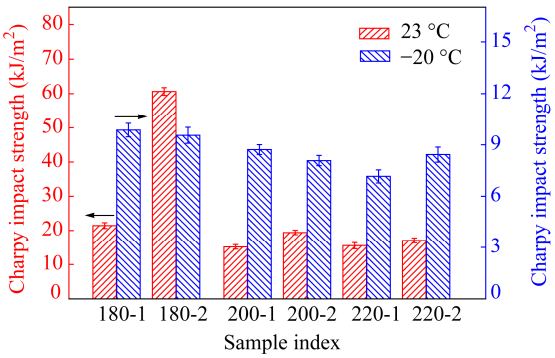


Fig. 9 Notched Charpy impact strength of IPC samples extruded at different temperatures

Shear Energy in Twin Screw Extruder

Since the core-shell particles in IPC can only be rebuilt in appropriate conditions by multiple extrusions, how to evaluate the shear or thermal effect quantitatively and how to obtain an appropriate processing condition are interesting and important issues.

The study on co-rotating twin screw extruder has made a great progress in past years, many researchers[43, 44] have proposed some complicated mathematical models to simulate the processing in twin screw extruder. However, due to the complexity of the flow channel determined by the geometry of screws, obtaining the shear rate in the screw extruder is an intricate issue for researchers not professional in the field of screw extruder. In this work, an equivalent method[45] is adopted to calculate the shear rate in extruder due to its

simplicity by equaling the flow channel of twin screw extruder to that of single screw extruder. Booy[43] gave the barrel and twin screw footprints as developed into a plane, as shown in Fig. S6(a) (seen in the Supporting Information), in which D_s stands for screw diameter and φ, ψ stand for helix angle, engaging angle, respectively. Disregarding the engaging area and in the case of unchanged helix angle, the flow channel of a twin screw can be equivalent to that of a single screw, as shown in Fig. S6(b)[45]. Consequently, the equivalent diameter of single screw can be expressed as the following form[45]

$$D_E = 2D_s\left(1-\frac{\psi}{\pi}\right) \tag{1}$$

in which D_E stands for the equivalent diameter. For single screw extruder, the mean shear rate in the channel is given by[46]

$$\dot{\gamma} = \frac{\pi ND}{H} \tag{2}$$

where $\dot{\gamma}$ stands for the mean shear rate, N stands for rotation speed of screw, D stands for screw diameter of single screw extruder which can be replaced by D_E here, and H stands for channel depth.

Tadmor and Gogos[47] have estimated the amount of energy needed by the processing of extruder. They pointed out that the power required for drag flow is a function of shear rate, internal free volume of extruder and viscosity. The function can be expressed as[47]

$$G = V\eta\dot{\gamma}^2 \tag{3}$$

in which G stands for the total power, V stands for the internal free volume of extruder and η stands for viscosity of polymer. However, the shear rates in the region of channel and in the top of thread are of great difference. Calculation of the total power should be divided into two parts, one is the region of channel and the other is the top of thread. Consequently, deducting the feed zone and ignoring the influence of mixing element, it is suggested that the shear energy per unit mass in extruder for non-Newtonian fluid can be expressed as the following form

$$E = \frac{(V_c K\dot{\gamma}_c^{n+1} + V_o K\dot{\gamma}_o^{n+1})t}{(V_c+V_o)\rho} \tag{4}$$

in which K stands for consistency coefficient which is dependent on temperature strongly, n is non-Newtonian index, t is residence time of polymer in extruder, ρ is density of polymer and subscripts c and o represent regions of channel and top of thread, respectively. Using the geometric parameters of screws, *i.e.*, screw diameter (15.6 mm), channel depth (3.3 mm), barrel bore diameter (16 mm), centre-line spacing (12.5 mm), volume of the channel (57.24 cm^3), volume of the top of thread (0.76 cm^3) and K, n obtained by rheological measurements at different temperatures (shown in the Supporting Information), the shear rate in extruder and shear energy per unit mass can be calculated as shown in Fig. 10.

As mentioned above, it is confirmed that the core-shell particle is unstable and could be destroyed during annealing. The system should reach an equilibrium state as long as the annealing time is long enough. Consequently, it is reasonable to infer that IPC with core-shell particles is in possession of a higher internal energy than the system with destroyed core-shell particles. However, in order to rebuild the core-shell particles again, it needs extra energy to offset the loss of internal energy. On the other hand, the shear rate associated with the rotation speed of screw required by the polymer should reach an optimal point since low shear rate could not change the structure of polymer melt with high viscosity. Furthermore, the viscosity of polymer concerned with temperature and shear rate should be opportune since the preservation of structure during solidification after extrusion needs a relatively high viscosity. In summary, it is concluded that when the shear rate and viscosity of polymer both reach the opportune values, the core-shell particles can be rebuilt with the provision of opportune

energy. Moreover, the internal energy in the possession of the core-shell particles can be determined as 66.58 J/g.

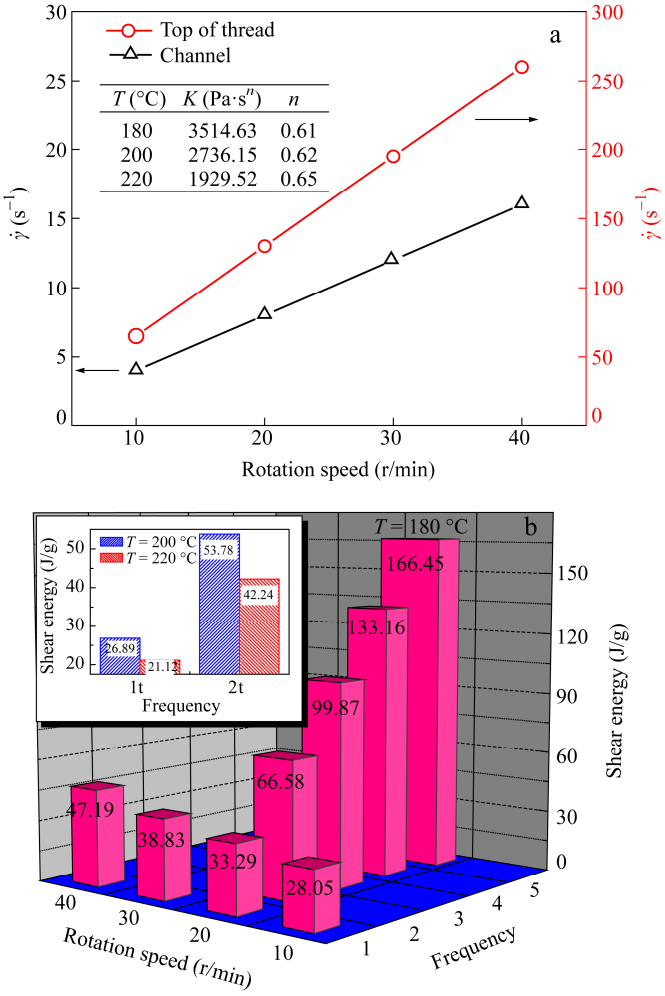


Fig. 10 (a) Shear rates in extruder and *K*, *n* of IPC at different temperatures and (b) shear energy at different extrusion conditions

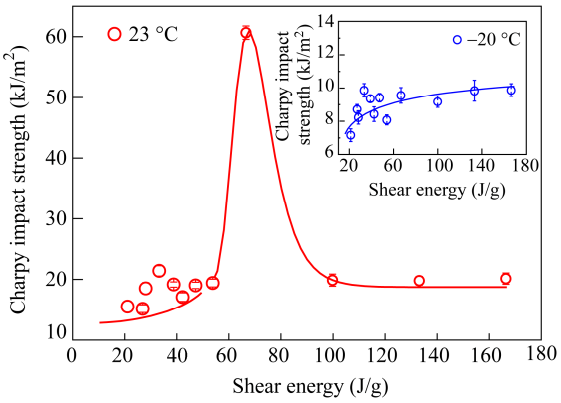


Fig. 11 Shear energy dependence of notched Charpy impact strength

In order to demonstrate the relationship between toughness and shear energy, Figure 11 shows the shear energy dependence of impact strength. However, the impact strength first increases slightly and after a huge elevation it drops to reach a constant with the increasing of shear energy at 23 °C. As for toughness at –20 °C, the impact strength increases slowly and reaches a constant quickly. Considering the results above, it is proposed that only in the case of appropriate shear energy, *i.e.* about 66.58 J/g, the core-shell dispersed particle can be rebuilt with the recovery of impact strength.

CONCLUSIONS

The molten-state annealing results revealed that the core-shell structure could be destroyed and consequently the impact strength dropped quickly due to the destruction of core-shell structure and the coarsening of rubbery phase. Through co-rotating twin screw extrusion, the dispersed particle with core-shell structure was reproduced at appropriate conditions due to the huge interfacial tension during solidification and the great difference in viscosity of components with the recovery of excellent impact strength. Faster extrusion speed and higher extrusion frequency could result in the destruction of the dispersed particle with core-shell structure once again and only an ordinary dispersed structure with small size of dispersed particles could occur. The impact strength results at room temperature revealed that only in case of the appropriate shear energy, the toughness of IPC could recover due to the reconstruction of core-shell dispersed particles. Contrarily, the impact strength at lower temperatures seems to be independent of the core-shell structure of dispersed particles and reaches a constant quickly with increasing the shear energy. Moreover, the internal energy in the possession of the core-shell particles can be determined as 66.58 J/g.

REFERENCES

1 Greco, R., Mancarella, C., Martuscelli, E., Ragosta, G. and Jinghua, Y., Polymer, 1987, 28(11): 1929
2 D'orazio, L., Mancarella, C., Martuscelli, E. and Sticotti, G., J. Mater. Sci., 1991, 26(15): 4033
3 McNally, T., McShane, P., Nally, G.M., Murphy, W.R., Cook, M. and Miller, A., Polymer, 2002, 43(13): 3785
4 Zhang, X.F., Xie, F., Pen, Z.L., Zhang, Y., Zhang, Y.X. and Zhou, W., Eur. Polym. J., 2002, 38(1): 1
5 Zhang, Q.X., Yu, Z.Z., Xie, X.L. and Mai, Y.W., Polymer, 2004, 45(17): 5985
6 Lin, Y., Chen, H.B., Chan, C.M. and Wu, J.S., Macromolecules, 2008, 41(23): 9204
7 Lin, Y., Chen, H.B., Chan, C.M. and Wu, J.S., J. Appl. Polym. Sci., 2012, 124(1): 77
8 Tjong, S.C. and Li, R.K.Y., J. Vinyl Addit. Technol., 1997, 3(1): 89
9 Labour, T., Vigier, G., Seguela, R., Gauthier, C., Orange, G. and Bomal, Y., J. Polym. Sci., Part B: Polym. Phys., 2002, 40(1): 31
10 Galli, P. and Haylock, J.C., Prog. Polym. Sci., 1991, 16(2–3): 443
11 Debling, J.A. and Ray, W.H., J. Appl. Polym. Sci., 2001, 81(13): 3085
12 Cheruthazhekatt, S., Pijpers, T.F.J., Harding, G.W., Mathot, V.B.F. and Pasch, H., Macromolecules, 2012, 45(4): 2025
13 Cheruthazhekatt, S., Pijpers, T.F.J., Harding, G.W., Mathot, V.B.F. and Pasch, H., Macromolecules, 2012, 45(15): 5866
14 Urdampilleta, I., Gonzalez, A., Iruin, J.J., de la Cal, J.C. and Asua, J.M., Macromolecules, 2005, 38(7): 2795
15 Chen, R.F., Shangguan, Y.G., Zhang, C.H., Chen, F., Harkin-Jones, E. and Zheng, Q., Polymer, 2011, 52(13): 2956
16 Tan, H.S., Xie, K., Liu, W.H., Hou, B., Shangguan, Y.G. and Zheng, Q., Acta Polymerica Sinica (in Chinese), 2006, (9): 1106
17 Song, S.J., Feng, J.C., Wu, P.Y. and Yang, Y.L., Macromolecules, 2009, 42(18): 7067
18 Song, S.J., Feng, J.C. and Wu, P.Y., Polymer, 2010, 51(22): 5267
19 Tan, H.S., Li, L., Chen, Z.N., Song, Y.H. and Zheng, Q., Polymer, 2005, 46(10): 3522
20 Rungswang, W., Saendee, P., Thitisuk, B., Pathaweeisariyakul, T. and Cheevasrirungruang, W., J. Appl. Polym. Sci., 2013, 128(5): 3131

21 Shangguan, Y.G., Zhang, C.H., Xie, Y.L., Chen, R.F., Jin, L. and Zheng, Q., Polymer, 2010, 51(2): 500
22 Zhang, C.H., Shangguan, Y.G., Tan, Y.Q., Chen, F., Huang, Z.Z. and Zheng, Q., Chemical Journal of Chinese Universities (in Chinese), 2012, 33(2): 430
23 Chen, Y., Chen, W. and Yang, D.C., Polymer, 2006, 47(19): 6808
24 Zhang, C.H., Shangguan, Y.G., Chen, R.F., Wu, Y.Z., Chen, F., Zheng, Q. and Hu, G.H., Polymer, 2010, 51(21): 4969
25 Chen, Y., Chen, W. and Yang, D.C., J. Appl. Polym. Sci., 2008, 108(4): 2379
26 Tong, C.Y., Lan, Y., Chen, Y., Yang, D.C. and Yang, X.N., J. Appl. Polym. Sci., 2012, 123(3): 1302
27 Jancar, J. and Tochacek, J., Polym. Degrad. Stab., 2011, 96(9): 1546
28 Tochacek, J., Jancar, J., Kalfus, J. and Hermanova, S., Polym. Degrad. Stab., 2011, 96(4): 491
29 Luo, F., Xu, C.L., Wang, K., Deng, H., Chen, F. and Fu, Q., Polymer, 2012, 53(8): 1783
30 Luo, F., Xu, C.L., Ning, N.Y., Wang, K., Deng, H., Chen, F. and Fu, Q., Polym. Int., 2013, 62(2): 172
31 Chen, Y., Chen, Y., Chen, W. and Yang, D.C., Eur. Polym. J., 2007, 43(7): 2999
32 Arvidson, S.A., Khan, S.A. and Gorga, R.E., Macromolecules, 2010, 43(6): 2916
33 Mamodia, M., Panday, A., Gido, S.P. and Lesser, A.J., Macromolecules, 2007, 40(20): 7320
34 Boulahia, R., Gloaguen, J.M., Zaïri, F., Naït-Abdelaziz, M., Seguela, R., Boukharouba, T. and Lefebvre, J. M., Polymer, 2009, 50(23): 5508
35 Modesti, M., Lorenzetti, A., Bon, D. and Besco, S., Polymer, 2005, 46(23): 10237
36 Beck, R.H., Gratch, S., Newman, S. and Rusch, K.C., J. Polym. Sci., Part B: Polym. Lett., 1968, 6(10): 707
37 Pavan, A. and Ricco, T., J. Mater. Sci., 1976, 11(6): 1180
38 Jang, B.Z., J. Appl. Polym. Sci., 1985, 30(6): 2485
39 Gardette, J.L., Sinturel, C. and Lemaire, J., Polym. Degrad. Stab., 1999, 64(3): 411
40 Philippart, J.L., Sinturel, C., Arnaud, R. and Gardette, J.L., Polym. Degrad. Stab., 1999, 64(2): 213
41 Qin, H.L., Zhang, S.M., Liu, H.J., Xie, S.B., Yang, M.S. and Shen, D.Y., Polymer, 2005, 46(9): 3149
42 Avella, M., Dellerba, R., Martuscelli, E. and Ragosta, G., Polymer, 1993, 34(14): 2951
43 Booy, M.L., Polym. Eng. Sci., 1980, 20(18): 1220
44 Jung, H. and White, J.L., Int. Polym. Proc., 2008, 23(3): 242
45 Wang, L. "The Study of High Performance Co-Rotating Twin-Screw Extruder and Devolatilization Mechanism" Ph.D. thesis, Beijing University of Chemical Technology, (November 1999)
46 Tadmor, Z. and Gogos, C.G., "Principles of Polymer Processing", 2nd ed., John Wiley & Sons, Inc., Hoboken, New Jersey, 2006
47 Todd, D.B., "Plastics Compounding: Equipment and Processing", 1st ed., Chemical Industry Press, Beijing, 2002